AGU PUBLICATIONS

Space Weather

RESEARCH ARTICLE
10.1002/2015SW001347

Key Points:
- SC caused by the extreme IP shock of 23 July 2012 is simulated
- GIC risk on low-latitude power grids is assessed
- GIC risk may reach "high" level for some equatorial power networks

Supporting Information:
- Animation S1

Correspondence to:
J. J. Zhang,
jjzhang@spaceweather.ac.cn

Citation:
Zhang, J. J., C. Wang, T. R. Sun, and Y. D. Liu (2016), Risk assessment of the extreme interplanetary shock of 23 July 2012 on low-latitude power networks, *Space Weather*, *14*, 259–270, doi:10.1002/2015SW001347.

Received 27 NOV 2015
Accepted 27 FEB 2016
Accepted article online 3 MAR 2016
Published online 22 MAR 2016

Risk assessment of the extreme interplanetary shock of 23 July 2012 on low-latitude power networks

J. J. Zhang[1], C. Wang[1], T. R. Sun[1], and Y. D. Liu[1]

[1]State Key Laboratory of Space Weather, National Space Science Center, Chinese Academy of Sciences, Beijing, China

Abstract Geomagnetic sudden commencements (SCs), characterized by a rapid enhancement in the rate of change of the geomagnetic field perturbation (d*B*/d*t*), are considered to be an important source of large geomagnetically induced currents (GICs) in middle- and low-latitude power grids. In this study, the extreme interplanetary shock of 23 July 2012 is simulated under the assumption that it had hit the Earth with the result indicating the shock-caused SC would be 123 nT. Based on statistics, the occurrence frequency of SCs with amplitudes larger than the simulated one is estimated to be approximately 0.2% during the past 147 years on the Earth. During this extreme event, the simulation indicates that d*B*/d*t*, which is usually used as a proxy for GICs, at a dayside low-latitude substation would exceed 100 nT/min; this is very large for low-latitude regions. We then assess the GIC threat level based on the simulated geomagnetic perturbations by using the method proposed by Marshall et al. (2011). The results indicate that the risk remains at "low" level for the low-latitude power network on a global perspective. However, the GIC risk may reach "moderate" or even "high" levels for some equatorial power networks due to the influence of the equatorial electrojet. Results of this study feature substantial implications for risk management, planning, and design of low-latitude electric power networks.

1. Introduction

Geomagnetically induced currents (GICs) in power networks exert a critical space weather threat to modern technological systems. The interaction between solar wind plasma and the Earth's magnetosphere produces highly variable magnetosphere-ionosphere current systems, inducing geoelectric fields in the ground and generating GICs in long-distance conductive ground infrastructures. The currents are at a low frequency (0.01–1 Hz) and flow through transformer windings, potentially saturating the core and leading to transformer malfunctions, permanent damage, or even collapse of the whole system [*Pirjola*, 2002]. The best known event demonstrating this was the Hydro-Québec blackout of March 1989 occurring during a large magnetic storm and leaving over 6 million people without power for 9 h [*Bolduc*, 2002]. Society and the economy have become significantly more dependent on electronic technology since then with new technologies relying on a stable supply of electrical power. Thus, the consequence of an extreme space weather event may be catastrophic. Estimates produced in a report by Lloyd's, a global insurance market, indicate that a Carrington-level space weather event could cause at least 20 million citizens lose power for a duration of up to 2 years in North America [*Jonas and McCarron*, 2015].

Initial studies of GICs were undertaken at high-latitude regions, where the ionospheric auroral electrojets during substorms are the most dominant source of GICs in power systems [*Boteler et al.*, 1982]. Substantial GICs have also been observed in middle- and low-latitude systems in recent years [*Kappenman*, 2003; *Gaunt and Coetzee*, 2007; *Liu et al.*, 2009; *Marshall et al.*, 2012]. Generally, the middle-latitude refers to latitudes between 30° and 60° in the Northern Hemisphere and latitudes between −30° and −60° in the Southern Hemisphere; the low-latitude refers to latitudes between −30° and 30°. Geomagnetic sudden impulses (SIs) and storm sudden commencements (SSCs), caused by the compression of the Earth's magnetosphere due to interplanetary (IP) shocks are considered, in addition to severe geomagnetic storms, as the core explanation for GICs in these power grids. *Kappenman* [2003] reported that a GIC measurement reached a peak of 130 A during the SSC event of 24 March 1991 in the Pleasant Valley substation (geomagnetic latitude ~52°) in the United States, which is located at the lower Hudson River valley in New York. The paper also reported the tripping of capacitor banks at some midlatitude American substations resulting from SSCs on 15 July 2000 and 31 March 2001. *Béland and Small* [2004] reported that a transformer accident occurred at the power

networks of New Zealand's South Island (geomagnetic latitude ~ −50°), which is associated with a SSC event on 6 November 2001. *Zhang et al.* [2015] reported GICs observed at two Chinese low-latitude high-voltage substations during the record storm of 17 March 2015, the largest storm of the present solar cycle to date [*Liu et al.*, 2015]. Observations by *Zhang et al.* [2015] indicate that GICs caused by the SSC were much higher than those in the storm main phase [*Zhang et al.*, 2015, Figure 3]. All of the events mentioned above suggest that the SSCs or SIs are important in inducing GICs in middle- and low-latitude power networks. In addition, the magnetic field signature of SSCs or SIs in the equatorial region may be amplified by the ionospheric equatorial electrojet, increasing the regions's susceptibility to GICs [*Carter et al.*, 2015]. In fact, the SSCs and SIs are caused by the same physical mechanism associating with the compression of the magnetosphere by IP shocks, the only difference is the *H* component enhancement is followed by a magnetic storm for SSCs [*Takeuchi et al.*, 2002; *Curto et al.*, 2007]. In this study we do not distinguish them and group them together as sudden commencement (SC) events as *Fiori et al.* [2014] did.

The response of the geospace environment to extreme space weather conditions as related to electric power supply impacts are of concern to the general space weather community and operators of electric power utilities. The major challenge to the task is the low frequency of the extreme events. There are not sufficient data to determine the statistical features of the response of the geospace environment [*Ridley et al.*, 2006]. An unusual solar storm with extremely strong solar wind speeds of 2246 km/s was observed on 23 July 2012 by NASA's STEREO A spacecraft, which at the time was located at 0.96 AU ahead of Earth in its orbit around the Sun [*Russell et al.*, 2013; *Cash et al.*, 2015]. *Liu et al.* [2014] suggested that the observed super solar storm was related to the in-transit interaction between two successive coronal mass ejections. The solar storm was fortunately not Earth directed. *Baker et al.* [2013] estimated that an extreme geomagnetic storm, potentially significantly larger than the famous Carrington storm of 1859, would have occurred under a "worst-case scenario" if this powerful solar storm had hit the Earth. This extreme event was then discussed as necessary to utilize as a model for severe space weather effects on technological systems. *Ngwira et al.* [2013a] applied the simulation results of the Space Weather Modeling Framework (SWMF) by utilizing the observations of STEREO A as the input of the model and calculated the possible geomagnetically induced electric fields at specific INTERMAGNET magnetometer sites. Their focus was on the influence of the possible strong geomagnetic storm; however, a much more detailed investigation of the 23 July 2012 event was indicated as necessary.

The IP shock prior to the extreme event of 23 July 2012 was exceptionally strong as the solar wind speed jumped from approximately 900 km/s to more than 2000 km/s across the shock. The extremely high solar wind speed of ~2000 km/s measured near 1 AU is very rare [*Evans et al.*, 2013]. These speeds have only previously been observed during the events of 4–5 August 1972 and 29–30 October 2003 [*D'uston et al.*, 1977; *Skoug et al.*, 2004]. The focus in this study is on the extreme IP shock and estimates for the resulting possible risk of GICs at low-latitude power networks if the shock impacted the Earth. Magnetospheric current systems will be checked before and after the extremely strong shock utilizing a global MHD model, and the amplitude of the resulting SC will be estimated. The resulting GICs will be calculated in a low-latitude power network and the threat level will be assessed. The trend of building long transmission lines to transport large amounts of electricity over great distances exposes the power networks to larger induced geoelectric field driving larger GICs [*Molinski*, 2002], such as the Chinese electricity transmission system assembled from west to east with nationwide power grid interconnection [*Zhou et al.*, 2010]. Power networks at low latitudes with this plan design are more vulnerable to GIC attacks than previously thought. Assessing risk under extreme conditions features critical applications for risk management of power networks and profound implications for planning and design of low-latitude power grids in the future.

2. Model and Method

2.1. The Global MHD Model and Data Source

The reaction of the magnetosphere to extreme interplanetary conditions is difficult to determine by statistical research, because the extreme events are infrequent. Therefore, it is necessary to turn to numerical models of the magnetosphere to determine the possible response of the magnetosphere environment to extreme interplanetary conditions [*Ridley et al.*, 2006]. Numerical models have been widely used in modeling extreme events [see, e.g., *Raeder et al.*, 2001; *Ridley et al.*, 2006; *Ngwira et al.*, 2014], but the validation of the models under extreme conditions is still a challenge with few events to test the model. The modeling process in this study is performed utilizing the global piecewise parabolic method with a Lagrangian remap (PPMLR)-MHD code developed by *Hu et al.* [2007]. The code has been utilized successfully in modeling the dynamic of the

magnetosphere-ionosphere system [*Wang et al.*, 2013]. Its ability in reproducing geomagnetic perturbations has been demonstrated by comparing the simulated results with space-based and ground-based observations [*Wang et al.*, 2010, 2011; *Zhang et al.*, 2012, 2015]. *Wang et al.* [2011], for example, demonstrated the model's ability to reproduce large-scale geomagnetic variations of the high-latitude region during a substorm. *Zhang et al.* [2012] showed that the model successfully simulated the geomagnetic variations at a transformer of the Finnish high-voltage power system and captured the main feature of the resulting GICs during a very strong storm of 1999. The results of *Zhang et al.* [2015] indicated the model's ability to accurately reproduce the main features of the SC prior to the strong storm of 17 March 2015 with particular precision for modeling the rate of change of geomagnetic perturbation (dB/dt) from which a satisfactorily accurate estimate of GICs is obtained. The works discussed above indicate that the PPMLR-MHD model is reliable for our applications.

The PPMLR-MHD code solves ideal MHD equations for the solar wind-magnetosphere-ionosphere coupling system. The solution domain is taken to be $-300\ R_E \le x \le 30\ R_E$, and $-150\ R_E \le y, z \le 150\ R_E$, where R_E is the radius of Earth. The number of simulation grids are 160 in the x direction and 162 in the y and z directions in GSM coordinates with the smallest grid spacing of $0.4\ R_E$. The inner boundary is typically set at $3\ R_E$ centered on the Earth for "normal" simulation, while in this study the inner boundary is set at $2\ R_E$ as the shock is sufficiently strong that the magnetopause is compressed especially close to the Earth. An electrostatic ionosphere is set at $1.017\ R_E$ (110 km); the ionospheric grid is 1° in latitude and 3° in longitude covering the high-latitude region down to a magnetic colatitude of 37°. Between the inner boundary and the ionosphere, there is a data gap region. Because near the Earth, higher resolution is required to model the converging field and high Alfvén wave speeds caused by the strong geomagnetic field need very small numerical time steps. This is computationally expensive and very difficult to solve in MHD code [*Yu et al.*, 2010]. In the gap region, the field-aligned currents (FACs) are mapped from the inner boundary along the Earth's dipole magnetic field lines to the ionosphere where they are used as a source term for the Poisson equation. Then the ionospheric potential is mapped back to the inner boundary to drive the convection velocity. The model is driven by solar wind conditions at the inflow boundary.

The STEREO mission consists of twin satellites in the heliospheric orbit with one ahead of Earth and the other trailing behind. The on-board instrument PLASTIC (Plasma and Suprathermal Ion Composition) observes the solar wind plasma and IMPACT (In situ Measurements of Particles And CME Transients) measures magnetic field data [*Galvin et al.*, 2008; *Luhmann et al.*, 2008]. Measurements from STEREO A, as presented by *Liu et al.* [2014], are adopted as inputs of the PPMLR-MHD model in this study. Figure 1 shows the interplanetary magnetic field (IMF) B_x, B_y, B_z, solar wind speed V_{SW}, plasma density N, and temperature T from 14:00 UT on 23 July 2012 to 04:00 UT on 24 July 2012. It should be noted that the measurements of proton density and temperature are largely missing across the shock because the conditions are beyond the ability of the detector. The density of electrons with energies larger than 45 eV times a factor of 5 was taken as a proxy of the proton density (because the core electrons below 45 eV cannot be measured). Similarly, the plasma temperature was derived from the observed solar wind speed, which is usually a good proxy of the solar wind proton temperature (except ejecta) [*Lopez*, 1987]. In simulation, we consider the V_{SW} as V_x and set V_y and V_z to 0; the IMF B_x is set to 0 to retain the divergence-free condition.

2.2. GICs Calculation Method

In order to obtain GICs, the geomagnetic perturbation at the power network is first determined. The modeled space currents of the magnetosphere-ionosphere coupling system including the magnetosphere currents, ionosphere currents, and FACs in the data gap region are employed to calculate geomagnetic variations on the ground by utilizing the Biot-Savart's law as follows:

$$\delta \boldsymbol{B}(\boldsymbol{R}) = \frac{\mu_0}{4\pi} \int_V \boldsymbol{J}(\boldsymbol{r}') \times \frac{\boldsymbol{R} - \boldsymbol{r}'}{|\boldsymbol{R} - \boldsymbol{r}'|^3} \mathrm{d}V \tag{1}$$

where $\boldsymbol{J}(\boldsymbol{r}')$ denotes the current source, $\boldsymbol{R}$ is the location of interest on the ground, $\boldsymbol{r}'$ is the position of the current source, and μ_0 is the magnetic permeability of free space. The detailed method to obtain FACs in the data gap region can be found in *Zhang et al.* [2013, 2014]. Contribution of the internal currents is also considered, which is roughly one third of the total geomagnetic perturbation [*Häkkinen et al.*, 2002].

Then the geoelectric field is calculated by using the plane wave method [*Cagniard*, 1953]. Based on the method, the x and y components of the geoelectric field $E_{x,y}$ can be computed from the perpendicular

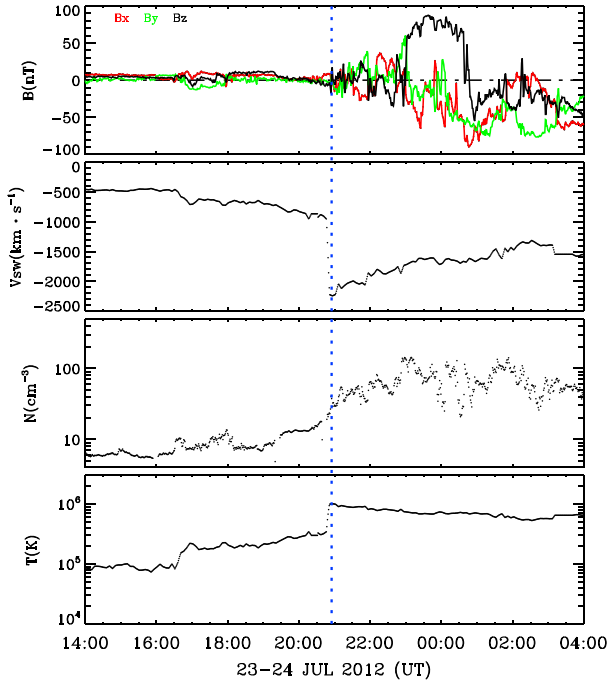

Figure 1. IMF and solar wind parameters during the extreme IP shock of 23 July 2012. From top to bottom, the panels show the IMF B_x, B_y, B_z, solar wind speed V_{SW}, plasma density N, and temperature T, respectively. The blue dashed line at 20:55 UT denotes the time of the IP shock.

geomagnetic perturbation components $B_{y,x}$, as follows:

$$E_{x,y} = \pm\frac{1}{\sqrt{\pi\mu_0\sigma}}\int_{-\infty}^{t}\frac{1}{\sqrt{t-u}}\frac{\mathrm{d}B_{y,x}(u)}{\mathrm{d}t}\mathrm{d}u \tag{2}$$

where the subscripts x and y denote north and east in geographic coordinates, respectively; σ is conductivity of the uniform ground. If we take the simplest assumption that the electric field is spatially uniform over the system region, geomagnetically induced currents can be calculated as follows:

$$GIC(t) = aE_x(t) + bE_y(t) \tag{3}$$

where a and b are constant coefficients, which are determined by the topology and electrical properties of the subject system. Parameters a and b can be deduced theoretically [*Lehtinen and Pirjola*, 1985] or deduced empirically by fitting the electric field and the corresponding GICs [*Pulkkinen et al.*, 2006; *Wik et al.*, 2008; *Zhang et al.*, 2012].

3. Results and Analysis

3.1. SC Caused by the Extreme IP Shock

The extreme IP shock was observed by the STEREO A spacecraft at 20:55 UT on 23 July 2012 [*Russell et al.*, 2013]. Illustrated in Figure 2 are cross sections of the magnetosphere's current density in the $Z = 0$ plane before (20:35 UT) and after (21:00 UT) the shock. The plots show the current density in color; note that the range of color bars is different for the two plots. Figure 2 indicates that the magnetosphere is highly compressed by the extreme IP shock. Across the shock, the location of the magnetopause nose moves from 6 R_E at 20:35 UT to 3.5 R_E at 21:00 UT with the increase of the maximum current intensity from 24 nA/m^2 to approximately 90 nA/m^2. The compression of the magnetopause by this IP shock is a bit weaker than the extreme "Carrington-type" space weather event modeled by *Ngwira et al.* [2014] using the three-dimensional SWMF model. *Ngwira et al.* [2014] showed that the dayside magnetophere is dramatically pushed to about 2.5 R_E by the greatly increased solar wind dynamic pressure.

To obtain the amplitude of the resulting geomagnetic SC event, we calculate the geomagnetic perturbations at four points which are distributed evenly at the Earth's equator and average the geomagnetic perturbations

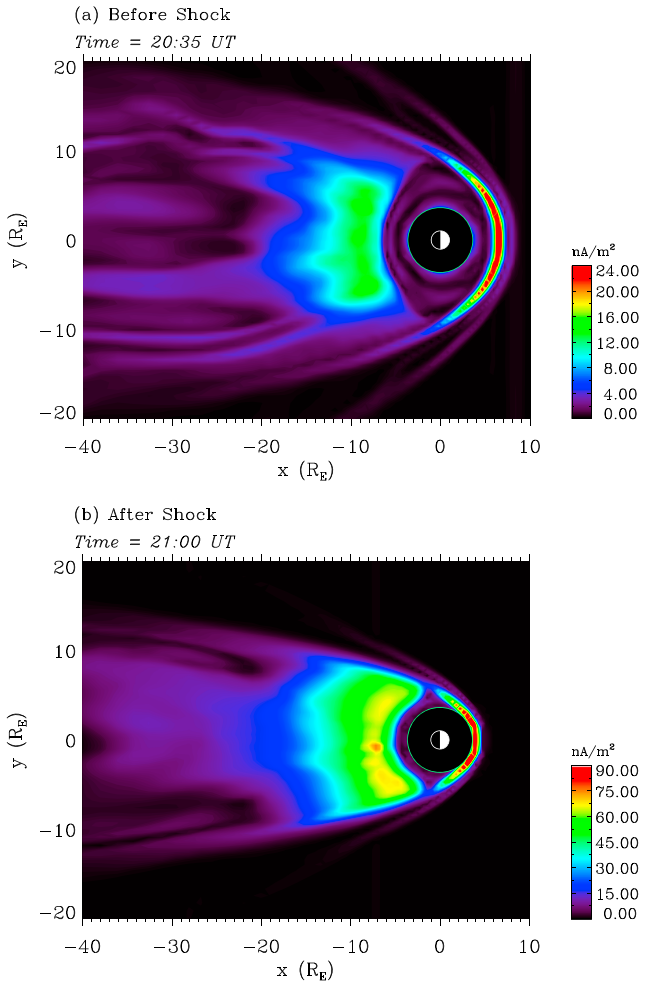

Figure 2. Simulated cross section of the magnetospheric current density in the $Z = 0$ plane (a) before and (b) after the extreme shock of 23 July 2012. The plots show the current density in color; note that the range of color bars is different for the two plots.

at these points as the simulated *SYM-H* index. The rapid increase of the simulated *SYM-H* during the IP shock is considered as the amplitude of the SC event. In observation, the *SYM-H* index is obtained based on measurements at several low-latitude sites to avoid the effect of the equatorial electrojet. The simulation does not contain the equatorial electrojet; thus, geomagnetic perturbations data from the points at the equator are utilized. Figure 3 presents the simulated *SYM-H* index, from which we determine that the amplitude of the SC is approximately 123 nT. The blue dashed line at 20:55 UT denotes the time of the IP shock observed by STEREO A. The simulated *SYM-H* reaches a maximum after about 1.5 min, which is just the travel time of the

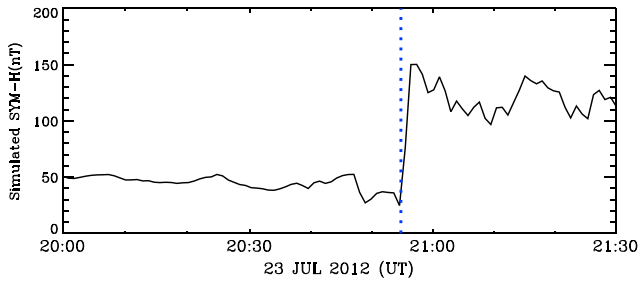

Figure 3. The simulated *SYM-H* index during the extreme IP shock of 23 July 2012, from which the SC amplitude is determined to be 123 nT. Blue dashed line at 20:55 UT denotes the time of the IP shock observed by STEREO A.

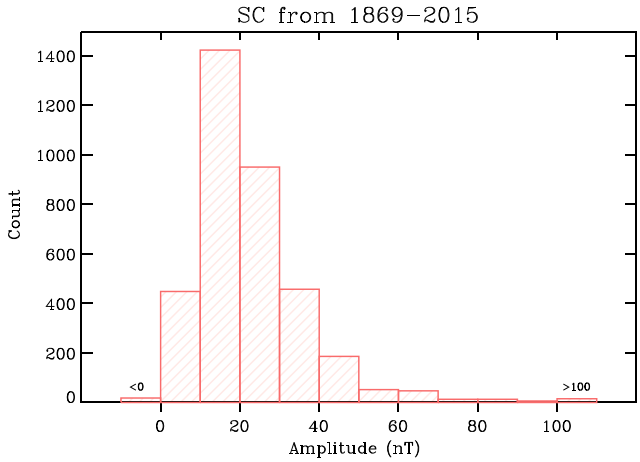

Figure 4. The histogram of SC amplitude distribution from year 1869 to 2015. SC events with amplitudes of less than 0 nT or more than 100 nT are grouped separately corresponding to the leftmost bin and rightmost bin in the plot, respectively.

shock from the inflow boundary (30 R_E) of the model to the Earth. The amplitude of the SC derived from our simulation is much larger than that derived from *Ngwira et al.* [2013a]. The simulated SC amplitude is about 30 nT in their study, which can be estimated from the simulated *SYM-H* index around 20:55 UT on 23 July 2012 in Figure 3a of their paper. We consider that the larger SC amplitude derived from our simulation result is mainly because the input solar wind density is much larger in our simulation. We use electrons with energies above 45 eV multiplied by a factor of 5 as a proxy of the solar wind density in this study, the plasma density increases from about 20 cm^{-3} to more than 40 cm^{-3} across the IP shock as shown in Figure 1. *Ngwira et al.* [2013a] used the beacon values of the solar wind density in their simulation. Across the shock, the density does not experience any change and the values do not rise above a few cm^{-3} during the whole event from 23 July to 24 July 2012, which was shown in the fifth panel of Figure 1 in their paper. Therefore, the solar wind dynamic pressure across the shock in our simulation is much stronger than that of *Ngwira et al.* [2013a]; this leads to a highly compressed magnetosphere and larger amplitude of the SC. *Baker et al.* [2013] states that the beacon values of the solar wind density highly underestimates the real solar wind conditions. So the amplitude of the SC is considered to be underestimated in the work of *Ngwira et al.* [2013a].

3.2. Occurrence Rate of Large SCs on the Earth

A statistical analysis is conducted to determine the rarity of exceptionally large SC events by considering the previously documented SC events. A list of SC events that have occurred since 1869 is maintained by the International Service on Rapid Magnetic Variations hosted by the Observatorio del Ebro (available at http://www.obsebre.es/en/rapid). From year 1869 to 2014, a total of 3612 SC events occurred excluding events with undetermined amplitude. In this study, to expand the data set to 2015, we identify 15 SC events during 2015 by analyzing *SYM-H* index maintained by the World Data Center for Geomagnetism, Kyoto (available at http://wdc.kugi.kyoto-u.ac.jp/). Therefore, there are 3627 SC events from 1869 to 2015 in our data set. The histogram of the SC amplitude distribution is presented in Figure 4. In the plot we divide the events with amplitudes between 0 nT and 100 nT into 10 groups with interval of 10 nT. The SC events with amplitudes of less than 0 nT or more than 100 nT are grouped separately because these events are seldom and their

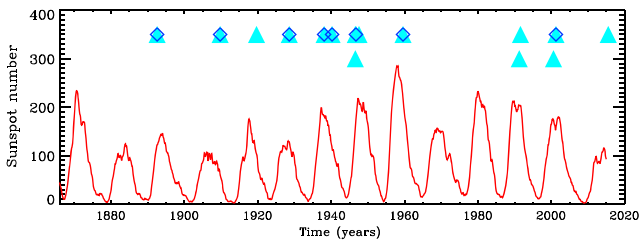

Figure 5. Solar activity and the occasions of large SC events from year 1869 to 2015. The occurrence of the SC events >100 nT are indicated by cyan triangles, and the SC events > 123 nT are indicated by blue diamonds.

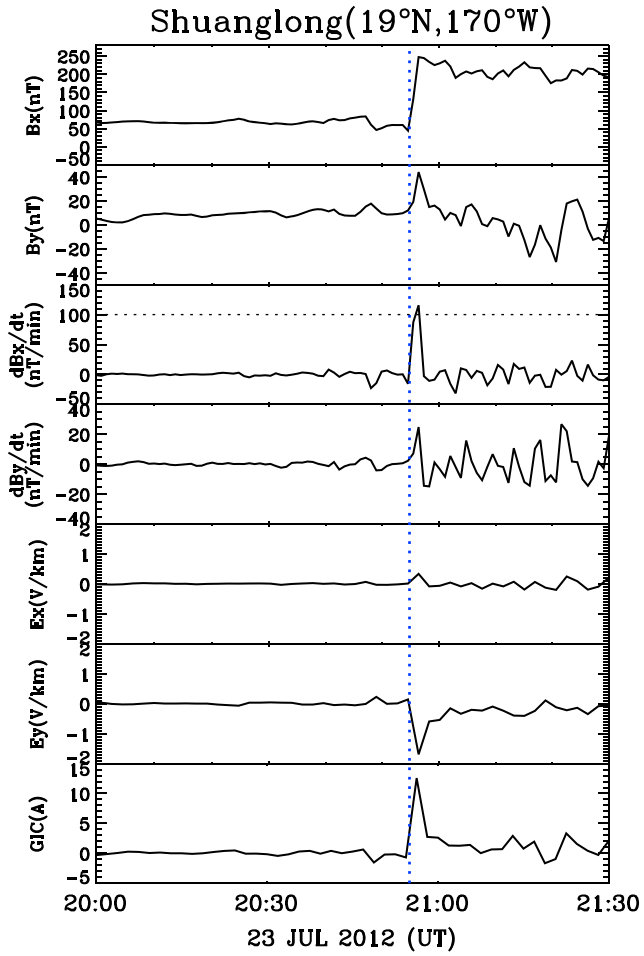

Figure 6. Simulation results for the Shuanglong 500 kV substation during the extreme IP shock of 23 July 2012. From top to bottom, the figure shows the *x* and *y* components of the geomagnetic variation B_x and B_y, time derivative of the geomagnetic variations dB_x/dt and dB_y/dt, induced geoelectric fields E_x and E_y, and GICs. The vertical blue dashed line at 20:55 UT denotes the time of the IP shock observed by STEREO A, and the black dashed line in the third panel indicates a dB_x/dt of 100 nT/min.

amplitude distribution is relatively disperse. The two groups correspond to the leftmost bin and rightmost bin in the plot, respectively. We can see from Figure 4 that typically, the amplitudes of the SC events are concentrated between 0 nT and 50 nT. The number of the SC events with larger amplitudes reduces rapidly. According to the statistics, the number of the SC events with amplitudes larger than 100 nT is 15 with an occurrence rate of less than 0.4% during the 147 year interval. There are eight SC events with amplitude larger than 123 nT; the occurrence rate is approximately 0.2%.

Figure 5 depicts the smoothed solar cycle and the occasions of large SC events from year 1869 to 2015. The 15 SC events with amplitudes larger than 100 nT are indicated by cyan triangles, and the 8 SC events with amplitudes larger than 123 nT are indicated by blue diamonds. The smoothed sunspot number is obtained from the Sunspot Index and Long-term Solar Observations (available at http://www.sidc.be/silso/datafiles). It is obvious from Figure 5 that the occurrences of the SC events with large amplitude are clustered in the years around the peak of each solar cycle, implying there is an increased risk of GICs.

We note that there is a large SC event that occurred on 31 March 2001. The amplitude of the SC is 124 nT; very close to that of the simulated SC event of 23 July 2012. By calculating the rate of change of *SYM-H* index ($d(SYM\text{-}H)/dt$) for the two events, we obtain that the maximum $d(SYM\text{-}H)/dt$ for the 31 March 2001 SC event is 60 nT/min, and that for the simulated SC event of 23 July 2012 is 74 nT/min. The NY-ISO (New York Independent System Operator, Inc.) reported the SC event of 31 March 2001 led to the tripping of a midlatitude capacitor bank which located at the East Fishkill (geomagnetic latitude ~52°) [*Kappenman*, 2003], which implies that the

simulated SC events may be also dangerous for midlatitude power networks since the rate of change of the *SYM-H* index for the simulated SC event of 23 July 2012 is larger than that for the SC event of 31 March 2001.

3.3. Risk Assessment of Low-Latitude Power Network

The Shuanglong 500 kV substation (geographic latitude ~29°, geomagnetic latitude ~19°) of China is taken as an example in this section to estimate the GIC risk level in a low-latitude power network under the assumption that the power network was located in the noon sector when the extreme IP shock swept across the Earth.

Parameters a and b in equation (3) for the Shuanglong 500 kV substation are $a = 8.33$ Akm/V and $b = -5.76$ Akm/V using a uniform Earth's conductivity of 0.0001 S/m, which have been obtained by utilizing the empirical method on the basis of geomagnetic variations and the GIC measurement in *Zhang et al.* [2015]. The assumption of a uniform Earth's conductivity of 0.0001 S/m is good enough since the cross-coefficients between the measured and fitted GICs was 0.94 and the normalized root-mean-square difference was 0.32 [*Zhang et al.*, 2015]. Figure 6 presents simulation results for the Shuanglong 500 kV substation during the extreme IP shock of 23 July 2012. The x and y components of the geomagnetic variation (B_x, B_y), time derivative of the geomagnetic variation (dB_x/dt, dB_y/dt), induced geoelectric field (E_x, E_y), and GICs are depicted from top to bottom in the figure. The geomagnetic perturbation is dominant in B_x at the Shuanglong substation and increases by approximately 200 nT under the impact of the extreme shock with the peak value of dB_x/dt exceeding 100 nT/min, which is exceptionally large for low-latitude regions. The increase in B_y is about 40 nT with a rate of change of 20 nT/min. In the analysis of 200 SC events which occurred from years 2000–2010, *Fiori et al.* [2014] indicated that nearly all the dB/dt observed at magnetometer stations located from −30° to 30° magnetic latitude, with the exception of the magnetic equator, were below 50 nT/min, which was shown in Figure 3c of their paper. In their study, B is the horizontal component of the magnetic field, $B = \sqrt{B_x^2 + B_y^2}$. A rate of change of the geomagnetic perturbation dB/dt of 100 nT/min is indicated as being especially rare for low-latitude locations. Figure 6 also shows the maximum geoelectric field E_y obtained is approximately −2 V/km. But the resulting GIC is then only 12.6 A, because the parameters a and b in equation (3) for the Shuanglong substation are relatively small. *Zhang et al.* [2015] considered that electric parameters and topology of the power systems render the Shuanglong substation less vulnerable to large GIC attacks through studying the GICs observed during the strong storm of 17 March 2015. During that SC event prior to the storm, B_x and B_y increased by 55 nT and 18 nT at the location of the substation, respectively, with a rate of change of the geomagnetic variations dB_x/dt of 40 nT/min and dB_y/dt of 9 nT/min. The peak of the induced geoelectric field were approximately 0.15 V/km and −0.45 V/km for E_x and E_y, respectively. The resulting GICs during the SC event was 4.5 A, which is much smaller than the simulated GICs due to the extreme event of 23 July 2012 considered in this study.

The magnitude of GICs and the tolerance capacity of transformers to GICs vary greatly for different power systems. They are highly dependent on the topology and electrical parameters of the particular power networks and the type of the transformers [*Pirjola*, 2005]. To assess the GIC threat level for power networks, *Marshall et al.* [2011] proposed a method to describe the risk level as a function of the GIC index, on the basis of the previously documented power network faults. They suggested that GIC_y indices of 50, 100, 250, and 600 correspond to lower limit thresholds for risk levels of "low," "moderate," "high," and "extreme," respectively. A frequency domain filter used in deducing the GIC index is given by the following:

$$Z(f) = \sqrt{\frac{f}{f_N}} e^{i\frac{\pi}{4}} \tag{4}$$

where f denotes frequency and f_N is the Nyquist frequency. The x and y components of geomagnetic field variation B_x and B_y are utilized to calculate the GIC_y and GIC_x index, respectively, as follows:

$$GIC_x(t) = \left|\mathrm{FFT}\{B_y(f)Z(f)\}^{-1}\right| \tag{5}$$

$$GIC_y(t) = \left|\mathrm{FFT}\{B_x(f)Z(f)\}^{-1}\right| \tag{6}$$

where $\mathrm{FFT}\{\}^{-1}$ denotes the inverse Fourier transform and $Z(f)$ is the filter function of equation (4). The method is applied in this study to derive the GIC_y index at the Shuanglong substation during the investigated event. Figure 7 demonstrates geomagnetic variation B_x at the Shuanglong substation and the associated GIC_y index

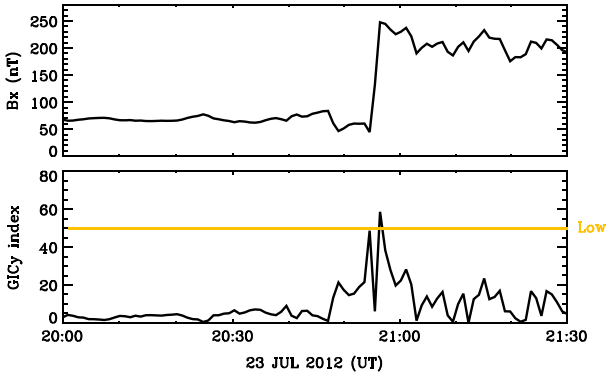

Figure 7. Geomagnetic variation B_x at the Shuanglong substation and the associated GIC_y index during the extreme IP shock of 23 July 2012. The golden horizontal line denotes a low GIC risk level.

with the golden horizontal line denoting a GIC_y index of 50. The figure indicates the Shuanglong substation is at low risk level under the influence of the extreme IP shock of 23 July 2012. This is not a surprise, because the GIC indices are derived from geomagnetic perturbations which are generally very low in the low-latitude region compared to the high-latitude regions. *Marshall et al.* [2011] utilized data from all latitude domains to rank threat levels, so the GIC indices at low-latitude regions are typically lower than at high-latitude regions. Nevertheless, dB_x/dt of 100 nT/min during this event is very high for the low-latitude region; and GICs impact to power systems were observed at levels lower than 100 nT/min [*Kappenman*, 2006]. As the length and scale of the electric power grids increases and development continues on the national interconnection strategy, the GIC flowing in low-latitude power networks of China may largely increase, enhancing the GIC risk level. It is therefore becoming necessary to develop a new kind of GIC risk index specially for the low-latitude regions.

3.4. Risk Assessment of Equatorial Power Network

The influence of the electrojet current on the local magnetic field is significant at the magnetic equator. *Pulkkinen et al.* [2012] and *Ngwira et al.* [2013b] suggested that the GIC enhancements at equatorial stations during large storms may be caused by the electrojet current. *Carter et al.* [2015] showed that the magnetic signal of the SC events could also be amplified by the electrojet current at the magnetic equator. The study indicated that due to the electrojet current effect, near local noon, the rate of change of the geomagnetic perturbation dB_x/dt caused by IP shocks can be 3 and 5 times that of d(*SYM-H*)/d*t* on average for the

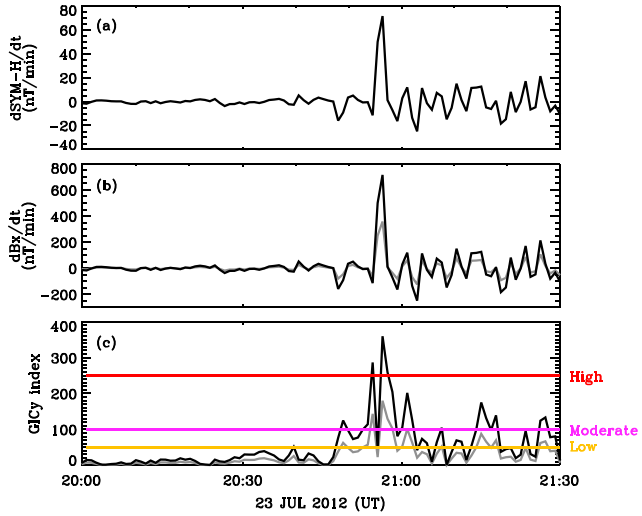

Figure 8. The rate of change of (a) simulated *SYM-H* index, (B) possible dB_x/dt at some equatorial location, and (c) the corresponding GIC_y index during the extreme IP shock of 23 July 2012. The grey curve in Figure 8b denotes the dB_x/dt which is 5 times of d(*SYM-H*)/d*t*, while the black curve denotes dB_x = d*t* of 10 times of d(*SYM-H*)/d*t*, and the corresponding GIC_y are indicated by grey and black curves, respectively, in Figure 8c. The golden, magenta, and red horizontal lines denote the low, moderate, and high GIC risk levels, respectively.

equatorial African and American stations, respectively. The amplification ratio $\frac{d}{dt}B_x/\frac{d}{dt}(SYM\text{-}H)$ can reach up to 10 for the American station, which was shown in Figure 2e of *Carter et al.* [2015]. The global MHD model employed in this study does not include the ionospheric model at the equatorial region; therefore, simulation of the electrojet current-induced GICs is not feasible. Here we just make a rough estimation of the risk level under the assumption that the dB_x/dt at some dayside equatorial station is 5 times (the common amplification ratio for the American station) of the simulated $d(SYM\text{-}H)/dt$ during the investigated event, or 10 times of $d(SYM\text{-}H)/dt$ in a worst-case scenario. Based on dB_x/dt, we calculate the GIC_y index by using the method described in section 3.3. The rate of change of *SYM-H* index during the extreme IP shock of 23 July 2013 is shown in Figure 8a and the possible rate of change of geomagnetic perturbation dB_x/dt which is 5 times of $d(SYM\text{-}H)/dt$ and 10 times of $d(SYM\text{-}H)/dt$ indicated by grey and black curves, respectively, are shown in Figure 8b. The corresponding curves of GIC_y index are shown in Figure 8c. The golden, magenta, and red horizontal lines denote the low, moderate, and high GIC risk levels, respectively, which are associated with GIC_y index of 50, 100, and 250. As Figure 8c shows, if the amplification ratio is 5, some power networks located at the magnetic equator region are then estimated to possibly reach moderate GIC risk level during the extreme IP shock of 23 July 2012. And the threat level can increase to high if the amplification ratio increases to 10 in a worst-case scenario.

4. Conclusion

Sudden commencement events associated with IP shocks are an important source of large GICs occurring at middle- and low-latitude power grids. The space weather community maintains significant concerns for the response of the geospace environment to extreme space weather conditions and the potential drastic impacts on electric power supply due to extreme space weather conditions. The SC event potentially resulting from the extreme IP shock of 23 July 2012, had it been Earth directed, is simulated in this study utilizing a global MHD model and considering STEREO A in situ observations as the inflow boundary condition driving the model. The simulation indicates that the amplitude of the resulting SC would be 123 nT. Analysis of previously documented SC events over 147 years reveals that large SC events with amplitudes greater than 123 nT are extraordinarily rare with an occurrence rate of approximately 0.2%. Occurrence of these events are clustered in the years around the peak of each solar cycle. Resulting GICs in a low-latitude substation of China is then estimated with the results indicating the GIC threat remains at a low level during the extreme IP shock from a global perspective. Rate of change of the geomagnetic perturbation dB_x/dt which is usually used as a proxy of GICs, however, would exceed 100 nT/min; this is infrequent and large at low-latitude locations during SC events. Previously reported equipment failures at midlatitudes for dB/dt levels of less than 100 nT [*Kappenman*, 2006] indicates the potential for hazardous conditions. GIC risk is estimated to potentially attain a high level for some power grids at the magnetic equatorial region during the extreme events as a result of the equatorial electrojet influence.

In this study, we focus on the GICs caused by an extreme IP shock. We examined a number of extreme events reported in previous studies and described the hypothetical GICs that could have been observed had the 23 July 2012 CME been earthward. GICs due to the ejecta could be much bigger and more sustained for the extreme event because the IMF southward components are extremely enhanced inside the ejecta and the speed is very high as well. Simulation results of *Ngwira et al.* [2013a] have shown that the modeled *SYM-H* index was comparable to previously observed severe geomagnetic storms such as the Halloween storm of 2003. The results in this study indicate that GICs due to extreme IP shocks might be very dangerous for low-latitude power networks.

Acknowledgments
We acknowledge the use of solar wind data from STEREO A. The sudden commencements list were obtained from the International Service on Rapid Magnetic Variations (http://www.obsebre.es/en/rapid), and the sunspot numbers were obtained from Sunspot Index and Long-term Solar Observations (http://www.sidc.be/silso/datafiles). We also thank the World Data Center for Geomagnetism, Kyoto, for using the *SYM-H* index. This work was supported by 973 Program2012CB825602, NNSFC grant 41404123, and in part by the Specialized Research Fund for State Key Laboratories of ChinaY42616A67S. The author J. J. Zhang is also supported by the Youth Innovation Promotion Association, Chinese Academy of Sciences.

References

Béland, J., and K. Small (2004), Space weather effects on power transmission systems: The cases of Hydro-Québec and Transpower New Zealand Ltd, in *Effects of Space Weather on Technology Infrastructure*, edited by I. A. Daglis, pp. 287–299, Springer, Netherlands.

Baker, D. N., X. Li, A. Pulkkinen, C. M. Ngwira, M. L. Mays, A. B. Galvin, and K. D. C. Simunac (2013), A major solar eruptive event in July 2012: Defining extreme space weather scenarios, *Space Weather*, *11*, 585–591, doi:10.1002/swe.20097.

Bolduc, L. (2002), GIC observations and studies in the Hydro-Québec power system, *J. Atmos. Sol. Terr. Phy.*, *64*(16), 1793–1802, doi:10.1016/S1364-6826(02)00128-1.

Boteler, D. H., T. Watanabe, R. M. Shier, and R. E. Horita (1982), Characteristics of geomagnetically induced currents in the BC Hydro 500 kV system, *IEEE Trans. Power Apparatus Syst.*, *PAS-101*(6), 1447–1456.

Cagniard, L. (1953), Basic theory of the magneto-telluric method of geophysical prospecting, *Geophysics*, *18*(3), 605–635.

Carter, B. A., E. Yizengaw, R. Pradipta, A. J. Halford, R. Norman, and K. Zhang (2015), Interplanetary shocks and the resulting geomagnetically induced currents at the equator, *Geophys. Res. Lett.*, *42*, 6554–6559, doi:10.1002/2015GL065060.

Cash, M. D., D. A. Biesecker, V. Pizzo, C. A. Koning, G. Millward, C. N. Arge, C. J. Henney, and D. Odstrcil (2015), Ensemble modeling of the 23 July 2012 coronal mass ejection, *Space Weather*, *13*, 611–625, doi:10.1002/2015SW001232.

Curto, J. J., T. Araki, and L. F. Alberca (2007), Evolution of the concept of sudden storm commencements and their operative identification, *Earth Planets Space*, *59*(11), i–xii.

D'uston, C., J. M. Bosqued, F. Cambou, V. V. Temny, G. Zastenker, O. L. Vaisberg, and E. G. Eroshenko (1977), Energetic properties of interplanetary plasma at the Earth's orbit following the August 4, 1972 flare, *Sol. Phys.*, *51*(1), 217–229.

Evans, R. M., A. A. Pulkkinen, Y. H. Zheng, M. L. Mays, A. Taktakishvili, M. M. Kuznetsova, and M. Hesse (2013), The score scale: A coronal mass ejection typification system based on speed, *Space Weather*, *11*(6), 333–334, doi:10.1002/swe.20058.

Fiori, R. A. D., D. H. Boteler, and D. M. Gillies (2014), Assessment of GIC risk due to geomagnetic sudden commencements and identification of the current systems responsible, *Space Weather*, *12*, 76–91, doi:10.1002/2013SW000967.

Galvin, A. B., L. M. Kistler, M. A. Popecki, C. J. Farrugia, K. D. C. Simunac, L. Ellis, E. Möbius, M. A. Lee, M. Boehm, and J. Carroll (2008), The plasma and suprathermal ion composition (PLASTIC) investigation on the STEREO observatories, *Space Sci. Rev.*, *136*(1–4), 437–486.

Gaunt, C. T., and G. Coetzee (2007), Transformer failures in regions incorrectly considered to have low GIC-risk, in *IEEE Lausanne Power Tech*, pp. 807–812, IEEE, Switzerland.

Häkkinen, L. V. T., T. I. Pukkinen, H. Nevanlinna, R. J. Pirjola, and E. I. Tanskanen (2002), Effects of induced currents on Dst and on magnetic variations at midlatitude stations, *J. Geophys. Res.*, *107*(A1), 1014, doi:10.1029/2001JA900130.

Hu, Y. Q., X. C. Guo, and C. Wang (2007), On the ionospheric and reconnection potentials of the Earth: Results from global MHD simulations, *J. Geophys. Res.*, *112*, A07215, doi:10.1029/2006JA012145.

Jonas, S., and E. D. McCarron (2015), Recent U.S. policy developments addressing the effects of geomagnetically induced currents, *Space Weather*, *13*, 730–733, doi:10.1002/2015SW001310.

Kappenman, J. G. (2003), Storm sudden commencement events and the associated geomagnetically induced current risks to ground-based systems at low-latitude and midlatitude locations, *Space Weather*, *1*(3), 1016, doi:10.1029/2003SW000009.

Kappenman, J. G. (2006), Great geomagnetic storms and extreme impulsive geomagnetic field disturbance events—An analysis of observational evidence including the great storm of May 1921, *Adv. Space Res.*, *38*(2), 188–199, doi:10.1016/j.asr.2005.08.055.

Lehtinen, M., and R. Pirjola (1985), Currents produced in earthed conductor networks by geomagnetically-induced electric fields, *Ann. Geophys.*, *3*(4), 479–484.

Liu, C. M., L. G. Liu, R. Pirjola, and Z. Z. Wang (2009), Calculation of geomagnetically induced currents in mid- to low-latitude power grids based on the plane wave method: A preliminary case study, *Space Weather*, *7*, S04005, doi:10.1029/2008SW000439.

Liu, Y. D., et al. (2014), Observations of an extreme storm in interplanetary space caused by successive coronal mass ejections, *Nat. Commun.*, *5*, 3481, doi:10.1038/ncomms4481.

Liu, Y. D., H. D. Hu, R. Wang, Z. W. Yang, B. Zhu, Y. A. Liu, J. G. Luhmann, and J. D. Richard (2015), Plasma and magnetic field characteristics of solar coronal mass ejections in relation to geomagnetic storm intensity and variability, *Astrophys. J. Lett.*, *809*, L34, doi:10.1088/2041-8205/809/2/L34.

Lopez, R. E. (1987), Solar cycle invariance in solar wind proton temperature relationships, *J. Geophys. Res.*, *92*(A10), 11,189–11,194.

Luhmann, J. G., D. W. Curtis, P. Schroeder, J. McCauley, R. P. Lin, D. E. Larson, S. D. Bale, J.-A. Sauvaud, C. Aoustin, and R. A. Mewaldt (2008), STEREO IMPACT investigation goals, measurements, and data products overview, *Space Sci. Rev.*, *136*(1), 117–184, doi:10.1007/s11214-007-9170-x.

Marshall, R. A., E. A. Smith, M. J. Francis, C. L. Waters, and M. D. Sciffer (2011), A preliminary risk assessment of the Australian region power network to space weather, *Space Weather*, *9*, S10004, doi:10.1029/2011SW000685.

Marshall, R. A., M. Dalzell, C. L. Waters, P. Goldthorpe, and E. A. Smith (2012), Geomagnetically induced currents in the New Zealand power network, *Space Weather*, *10*, S08003, doi:10.1029/2012SW000806.

Molinski, T. S. (2002), Why utilities respect geomagnetically induced currents, *J. Atmos. Sol. Terr. Phy.*, *64*(16), 1765–1778.

Ngwira, C. M., A. Pulkkinen, M. Leila Mays, M. M. Kuznetsova, A. Galvin, K. Simunac, D. N. Baker, X. Li, Y. Zheng, and A. Glocer (2013a), Simulation of the 23 July 2012 extreme space weather event: What if this extremely rare CME was Earth directed?, *Space Weather*, *11*, 671–679, doi:10.1002/2013SW000990.

Ngwira, C. M., A. Pulkkinen, F. D. Wilder, and G. Crowley (2013b), Extended study of extreme geoelectric field event scenarios for geomagnetically induced current applications, *Space Weather*, *11*, 121–131, doi:10.1002/swe.20021.

Ngwira, C. M., A. Pulkkinen, M. M. Kuznetsova, and A. Glocer (2014), Modeling extreme "Carrington-type" space weather events using three-dimensional global MHD simulations, *J. Geophys. Res.*, *119*, 4456–4474, doi:10.1002/2013JA019661.

Pirjola, R. (2002), Review on the calculation of surface electric and magnetic fields and of geomagnetically induced currents in ground-based technological systems, *Surv. Geophys.*, *23*(1), 71–90.

Pirjola, R. (2005), Effects of space weather on high-latitude ground systems, *Adv. Space Res.*, *36*(12), 2231–2240, doi:10.1016/j.asr.2003.04.074.

Pulkkinen, A., A. Viljanen, and R. Pirjola (2006), Estimation of geomagnetically induced current levels from different input data, *Space Weather*, *4*, S08005, doi:10.1029/2006SW000229.

Pulkkinen, A., E. Bernabeu, J. Eichner, C. Beggan, and A. W. P. Thomson (2012), Generation of 100-year geomagnetically induced current scenarios, *Space Weather*, *10*, S04003, doi:10.1029/2015SW000750.

Raeder, J., Y. L. Wang, T. J. Fuller-Rowell, and H. J. Singer (2001), Global simulation of space weather effects of the Bastille day storm, *Sol. Phys.*, *204*, 325.

Ridley, A. J., D. L. Zeeuw, W. B. Manchester, and K. C. Hansen (2006), The magnetospheric and ionospheric response to a very strong interplanetary shock and coronal mass ejection, *Adv. Space Res.*, *38*, 263–272, doi:10.1016/j.asr.2006.06.010.

Russell, C. T., R. A. Mewaldt, J. G. Luhmann, G. M. Mason, T. T. von Rosenvinge, C. M. S. Cohen, R. A. Leske, R. Gomez-Herrero, A. Klassen, and A. B. Galvin (2013), The very unusual interplanetary coronal mass ejection of 2012 July 23: A blast wave mediated by solar energetic particles, *Astrophys. J.*, *770*(1), 38, doi:10.1088/0004-637X/770/1/38.

Skoug, R. M., J. T. Gosling, J. T. Steinberg, D. J. McComas, C. W. Smith, N. F. Ness, Q. Hu, and L. F. Burlaga (2004), Extremely high speed solar wind: 29–30 October 2003, *J. Geophys. Res.*, *109*, A09102, doi:10.1029/2004JA010494.

Takeuchi, T., T. Araki, A. Viljanen, and J. Watermann (2002), Geomagnetic negative sudden impulses: Interplanetary causes and polarization distribution, *J. Geophys. Res.*, *107*(A7), 1096, doi:10.1029/2001JA900152.

Wang, C., T. R. Sun, X. C. Guo, and J. D. Richardson (2010), Case study of nightside magnetospheric magnetic field response to interplanetary shocks, *J. Geophys. Res.*, *115*, A10247, doi:10.1029/2010JA015451.

Wang, C., J. J. Zhang, B. B. Tang, and S. Y. Fu (2011), Comparison of equivalent current systems for the substorm event of 8 March 2008 derived from the global PPMLR-MHD model and the KRM algorithm, *J. Geophys. Res.*, *116*, A07207, doi:10.1029/2011JA016497.

Wang, C., X. C. Guo, Z. Peng, B. B. Tang, T. R. Sun, W. Y. Li, and Y. Q. Hu (2013), Magnetohydrodynamics (MHD) numerical simulations on the interaction of the solar wind with the magnetosphere: A review, *Sci. China Earth Sci.*, *56*(7), 1141–1157, doi:10.1007/s11430-013-4608-3.

Wik, M., A. Viljanen, R. Pirjola, A. Pulkkinen, P. Wintoft, and H. Lundstedt (2008), Calculation of geomagnetically induced currents in the 400 kV power grid in southern Sweden, *Space Weather*, *6*, S07005, doi:10.1029/2007SW000343.

Yu, Y. Q., A. J. Ridley, D. T. Welling, and T. Gabor (2010), Including gap region field-aligned currents and magnetospheric currents in the MHD calculation of ground-based magnetic field perturbations, *J. Geophys. Res.*, *115*, A08207, doi:10.1029/2009JA014869.

Zhang, J. J., C. Wang, and B. B. Tang (2012), Modeling geomagnetically induced electric field and currents by combining a global MHD model with a local one-dimensional method, *Space Weather*, *10*, S05005, doi:10.1029/2012SW000772.

Zhang, J. J., C. Wang, B. B. Tang, and H. Li (2013), Effect of the solar wind conditions on the ionospheric equivalent current systems, *Ann. Geophys.*, *31*(3), 489–501, doi:10.5194/angeo-31-489-2013.

Zhang, J. J., C. Wang, and B. B. Tang (2014), Improved method to derive equivalent current systems from global MHD simulations, *Sci. China Earth Sci.*, *57*(1), 167–173, doi:10.1007/s11430-013-4631-4.

Zhang, J. J., C. Wang, T. R. Sun, C. M. Liu, and K. R. Wang (2015), GIC due to storm sudden commencement in low-latitude high-voltage power network in China: Observation and simulation, *Space Weather*, *13*, 643–655, doi:10.1002/2015SW001263.

Zhou, X., J. Yi, R. Song, X. Yang, Y. Li, and H. Tang (2010), An overview of power transmission systems in China, *Energy*, *35*(11), 4302–4312, doi:10.1016/j.energy.2009.04.016.